# In-vitro studies of betamethasone/cyclodextrin inclusion complexes

K. Al-Sou'od[1,*], M. Al-Enazi[1], R. Ghanem[1] and R. Abuflaha[1]

[1]*Department of Chemistry, Al al-Bayt University, Mafraq, Jordan*
*P.O. Box 130040, Mafraq 25113, Jordan. Tel.: +962 79 5861350; fax: +962 2 6297025*
***Corresponding author**: khaldoun@aabu.edu.jo

**ABSTRACT** The interaction of Betamethasone (BMTZ) with different types of cyclodextrins (CD) was investigated. The effects of the types and concentration of CDs, as well as temperature on the inclusion behavior were also investigated. Different techniques were used in this investigation including phase solubility diagram (PSD), differential scanning calorimetry (DSC), scanning electron microscope (SEM), $^1$H-NMR and molecular mechanics (MM). PSD results indicated that the tendency of BMTZ to bind to CDs follows the order $\gamma$-CD < $\alpha$-CD < HP-$\beta$-CD < $\beta$-CD. This provides indications that size fit plays an important role on the inclusion complexation process. The thermodynamic parameters of the inclusion complexes under investigation were calculated. The negative entropy change indicated that con-formational changes were the dominant compared to the release of water solubility for the CD cavity and these formed an ice-burg structure around the BMTZ. MM study revealed that the dominant driving force of the inclusion complexation is the electrostatic energy. The DSC and SEM confirmed the for-mation of inclusion complex in the solid state.

**KEYWORDS** Volatile flavour compounds of shalgam; Shalgam quality; Ethyl acetimidate; Storage

## 1. Introduction

Cyclodextrins (CDs) are well-known cyclic oligosaccharides that are composed of $\alpha$-1, 4-linked gluc]'ojopyranose constituents (Malaekeh-Nikouei et al., 2007). The three most common CDs have 6, 7, and 8 glucopyranose units in their macrocycle and are called $\alpha$-CD, $\beta$-CD, and $\gamma$-CD, respectively (Szejtli, 1998; Misiuk and Zalewska, 2009). CDs have been used intensively to bolster the biological adequacy of complexes and provides increased solubility and stability in inclusion complexes. The magnitudes of the aperture, which are about 6, 8, and 10 Å for $\alpha$-CD, $\beta$-CD, and $\gamma$-CD, respectively are dissimilar. The aperture's depth for the CDs is approximately 8 Å. CDs have a truncated cone-shaped macrocycles known for their inner hydrophobic and outer hydrophilic surface because of their unique chemical structure. The hydrophobic accessible internal aperture creates non-covalent guest-host complex with an extensive heterogeneity of natural and artificial molecules of appropriate shape and size (Jansook et al., 2018). The incorporation of natural compounds inside the CD hydrophobic aperture significantly influences the physicochemical features of the guest molecules, such as solubility, stability and bioavailability (Cheng et al., 2015; Ravishankar and Dhamodharan, 2020). The complex chemically bonded atoms can be completely or partly encapsulated in CDs cavities. Numerous investigations have concentrated on the capability of CDs to encapsulate guests of different magnitudes in varied stoichiometric ratios. Depending on the host (CD) and guest sizes, different host-guest stoichiometric ratios are possible in the complex (Miao et al., 2017). The inclusion complexes of $\beta$-CD and HP-$\beta$-CD with antidiabetic new drugs have been studied by Uria-Canseco et al. (2019) it was suggested the formation a 1:1 complexes as characterized by Isothermal Titration Calorimetry. The interaction between some CD's and ethinyloestradiol were investigated and characterized spectrophotometrically and via MM (Uria-Canseco et al., 2019). Phase solubility studies suggested the formation of 1:1 stoichiometric inclusion complex of cholesterol with $\beta$-CD (Dai et al., 2022). Betamethasone was selected as the replica medication owing to its recognized capability to produce inclusion complexes with several cyclodextrins (Flood et al., 2000; Otagiri et al., 1984; Gillet et al., 2009).

Snow et al employed HPLC to study the inclusion complexes formed between various CDs and a sequence of corticosteroids related to BMTZ. They found that stronger inclusion complexes were achieved with $\gamma$-CD and HP-$\gamma$-CD compared to $\beta$-CD and its derivatives. The influence of multiple CDs on the water solubility of BMTZ and the sheath efficacy in liposomes were investigated employing PSD. Franz diffusion cells were employed to investigate BMTZ delivery kinetics (Flood et al., 2000). Piel et al. (2006) studied the effect of different CDs on the solubility of BMTZ using PSD. They found that BMTZ can form very stable molecular complexes with HP-$\gamma$-CD, Crysmeb, HP-$\beta$-CD and Rameb (Piel et al., 2006). Figure 1 presents the structure of betamethasone. BMTZ has a low oral bioavailability attributable primarily to its poor solubility in aqueous solution. Defectively water- solubility medicines are still a challenge, but they are nonetheless an imperative category of pharmaceutical compounds for the cure of a broad spectrum of illnesses. Different methods have been employed to navigate a panacea for this challenge culminating in silico and in vitro assessment of the


DOI: 10.52292/j.laar.2024.1105
Received: July 18, 2022.
Accepted: April 22, 2023.
Recommended by Diego Lomonaco.

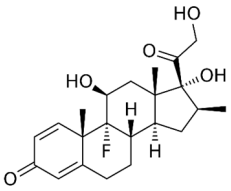


Figure 1: Chemical Structure of betamethasone.

production technologies for defectively water- solubility medications. The improvement approach for the solubility of defectively solubility drugs involves physicochemical modifications of the drug (Al-Sou'od, 2008; Boyd et al., 2019). In the present study, we hypothesized that complexation of BMTZ with CDs ($\alpha$-CD, $\beta$-CD, $\gamma$-CD, and HP-$\beta$-CD) will improve its solubility and biological stability. Our objective was to explore the robustness of the complexes as well as obtain information about their stoichiometry. Moreover, the influence of temperature on the stability of the inclusion complexes has been studied. The inclusion complexes under investigation have been characterized using spectroscopic (PSD and 1H-NM) and microscopic (SEM) techniques and have been further studied using computational methods (MM calculations).

## 2. Materials and methods

### 2.1 Materials

BMTZ was furnished by Al-Hikma Co (Jordan). $\alpha$-CD (99.3 %), $\beta$-CD (99.9 %) and $\gamma$-CD (98.7 %) were fabricated by Wacker Chemie (Germany), hydroxypropyl-$\beta$-CD (HP-$\beta$-CD with a 6.3 degree of substitution was fabricated by Yiming Fine Chemicals (China). The water used was distilled twice. The Jordanian Pharmaceutical Production Company (JPP) furnished the entire aforementioned stoichiometry materials. Other analytic class of chemicals were purchased from Merck (Germany) and Across Organic (Belgium).

### 2.2 Instruments

UV/Visible spectrophotometer (Du-650i, Beckman, USA). Thermostatic bath shaker (1086, GFL, Germany) connected to a chiller (23 DT 662-1, Heto-Holten, Denmark). pH-meter (744, Metrohm, Switzerland). Differential scanning calorimeter (910S, TA instrument, USA). Scanning electron microscope (Quanta 600, FEI, Netherlands) powered at an increasing electromotive force of 25 kV. NMR spectra were acquired with a Bruker Ultra Shield (Bruker-300MHz, Switzerland).

### 2.3 Phase solubility studies

Solubility investigations were carried out in line with Higuchi and Connors' earlier explanation (Higuchi 1965). A specific amount of BMTZ was introduced into 50 mL of 0.10 M phosphate buffer solutions (pH = 7.0) containing various concentrations of $\alpha$-CD, $\beta$-CD, $\gamma$-CD, and HP-$\beta$–CD (1–15 mM). The resultant solutions were shaken for 48 h in water bath (at $\sim$ 200 rpm) to achieve equilibrium and then left to settle for attainment of solubility equilibrium at the same temperature (25-40 °C); an aliquot was then filtered using a 0.45 mm membrane filter. The filtrates were diluted accordingly with the buffered solution at the same pH for measurement of the absorbance. An aliquot from each vial was sufficiently diluted and the chemical level of BMTZ was measured using a UV spectrophotometer at $\lambda_{max}$ of 240 nm with a predetermined standard curve. BMTZ/$\beta$-CD inclusion complex was confirmed by chemical analysis, which was done by collecting the precipitate from the descending portion of the PSD through suction filtration, and dried under vacuum for 24 h at ambient temperature. A suitable weight of the precipitate was dissolved in the phosphate buffer and analyzed by spectrophotometry for the stoichiometric determination of the absorbance. All experiments performed in triplicate. The apparent stability constants ($K_{app}$) of each BMTZ complex were computed from PSDs using the slope and the water solubility of BMTZ ($S_o$) in conformity with

$$K_{app} = \frac{slope}{S_o \cdot (1 - slope)} \quad (1)$$

### 2.4 Physical mixture preparation

Physical mixture of BMTZ and $\beta$-CD (molar ratio of 1:1) was made by combining the pulverized powder of each component, which was previously treated separately similarly to complex preparations in a ceramic mortar.

### 2.5 Physical mixture preparation

Inclusion complex of BMTZ and $\beta$-CD was made as described earlier.

### 2.6 Characterization of BMTZ /$\beta$-CD complex

#### 2.6.1 Differential Scanning Calorimetry (DSC)

Thermal behavior of BMTZ, $\beta$-CD, physical mixture, and inclusion complex were assessed using DSC (Perkin Elmer). The analysis was accomplished between 0 and 300 °C at a heating rate of 10 °C/min under nitrogen purging in a standard aluminum pan. An empty pan was employed as a reference.

#### 2.6.2 SEM Analysis

The surface morphology of BMTZ-$\beta$-CD inclusion complex was examined using a SEM (JSM-6510, SAI labs, TIET, Patiala, India) under 500 and 2000 magnifications. Preparation of samples were achieved by placing 0.5 mg of powder into a 5 mm$\times$5 mm silicon wafer attached through graphite (carbon) tap to an aluminum stub. This was followed by sputter-coating of the powder with a 100 Å layer of gold/palladium alloy for 40 s employing a beam current of 38-42 mA.

#### 2.6.3 $^1$H-NMR

The BMTZ and $\beta$-CD Nuclear Magnetic Resonance (NMR) spectra, physical mixture and BMTZ/$\beta$-CD complex were recorded in deuterated dimethyl sulfoxide (DMSO-d6) on an NMR spec-trometer using tetramethyl silane (TMS) as the internal standard. Chemical shift difference ($\Delta\delta$) was calculated employing the relation: $\Delta\delta = \delta$(complex) - $\delta$(free).

#### 2.6.4 Molecular Modeling (MM)

In order to elucidate the intermolecular interactions and calculate the interaction energies between BMTZ and CDs, we employed molecular modeling (MM) techniques.

MM investigations were carried out in vacuum to forecast the generation of BMTZ/CD inclusion complexes and to measure their binding affinity employing Hyperchem® (release 8.06). Force fields used in these computations were Amber94, enhanced MM, BIO+ (CHARMM) and OPLS method actualized in Hyperchem using the atomic charges or bond dipoles options for calculation of electrostatic interactions. Bond, angle, torsion, non-bonded, electrostatic and hydrogen-bonded interactions were calculated for all types of force fields. Partial atomic charges were achieved through AM1 semi-empirical calculations and the amount of charge on each atom (total number of BMTZ atoms was 57) was assigned.

Energy minimizations were achieved employing Polak-Rebiere algorithm (0.1 kcal/mol.A) gradient. The starting geometries of CDs ($\alpha$-CD, $\beta$-CD and $\gamma$-CD) were achieved employing X-ray diffraction data (Al-Sou'od, 2008). The Amber force field was employed to further optimize these geometries by imposing a restraint on the dihedral angles and the average values. HP-$\beta$-CD was generated by manually attaching randomly isopropyl groups to the primary hydroxyls (6.3 degree of substitution). BMTZ was developed from natural bond angles as defined in this software. The structures were then minimized with the MM, Amber, BIO+ (CHARMM) and OPLS force field, and the resulting structure was further optimized at the HF-ab initio level with the 3-21G basis set (310 basis functions were used with 507 primitive Gaussians).

## 3. Results

Due to the low water solubility and chemical stability of BMTZ, the bioavailability of BMTZ is low and let to reduce its clinical application. To improve its aqueous solubility, stability and pharmacological effects, BMTZ was complexed with $\beta$-CD. It was observed that due to formation of the inclusion complex, the aqueous solubility of BMTZ was enhanced.

### 3.1 Influence of CD type

Complex generation constants ($K_{ij}$) were estimated by analyzing PSDs using rigorous procedures described earlier (Zughul and Badwan, 1998; Zughul, 2007). Rigorous nonlinear regression of experimental data corresponding to each phase diagram was utilized to obtain estimates of $K_{ij}$ (Zughul and Badwan, 1998; Zughul, 2007).

Figure 2 depicts phase solubility diagrams (PSDs) obtained for BMTZ against $\alpha$-, $\beta$- HP-$\beta$- and $\gamma$-CD concentration in 0.1 M, 0.10 M NaCl phosphate buffers (pH = 7.0) and a temperature of 25 °C. The variations in the solubility curves can clearly be seen in the figure. The solubility of BMTZ increased with increasing $\alpha$-, $\beta$- HP-$\beta$- and $\gamma$-CD concentrations. The outcomes demonstrated the generation of 1:1 BMTZ/CD complexes with all kinds of CD. BMTZ forms two types of phase solubility diagrams based on the findings of our investigation. BMTZ forms $A_L$ type solubility curve with $\alpha$-, HP-$\beta$- and $\gamma$-CD. This type of diagram indicates that the solubility of BMTZ increased linearly with the increase in CD concentration, contingent upon the water solubility of the CD (Higuchi, 1965). PSD obtained for the BMTZ/$\beta$-CD in phosphate buffer solution can be classified as $B_s$ type. This type of phase solubility diagram originates from a rising portion followed by a plateau region and a decrease in BMTZ concentration, with a microcrystaline complex precipitation at high $\beta$-CD con-centration (11 mM). The predicted equilibrium solubility $S^P_{eq}$ can be estimated from nonlinear least square fitting of experimental data as described in our work (Al-Sou'od, 2008).

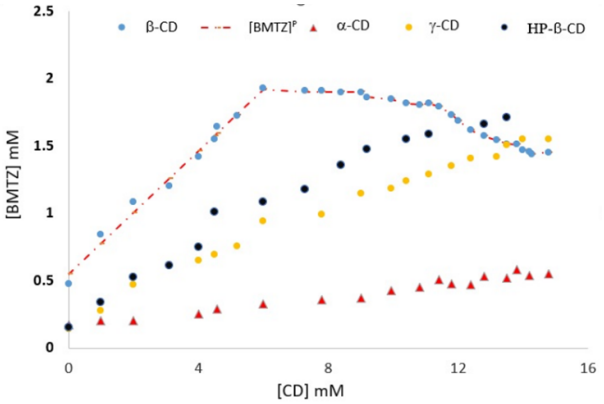


Figure 2: Phase solubility diagrams of the BMTZ/CD systems in 0.1 M phosphate buffer (pH 7.0) at 25 °C.

Table 1: Values of $K_{1:1}$ and $K_{app}$ of the BMTZ/CD system achieved in 0.1 M phosphate buffer (pH 7.0) and varied temperatures.

| Host | Temp °C | $S_o$ (mmolL$^{-1}$) | $K_{1:1}$ (Lmol$^{-1}$) | $R^2$ | $K_{app}$ (Lmol$^{-1}$) |
|---|---|---|---|---|---|
| $\alpha$-CD | 25 | 0.29 | 166.3 | 0.9757 | 164.7 |
| | 30 | 0.36 | 153.0 | | 144.2 |
| | 35 | 0.42 | 106.3 | | 91.2 |
| | 40 | 0.53 | 85.0 | | 85.8 |
| $\beta$-CD | 25 | 0.22 | 1350.7 | 0.9858 | 798.6 |
| | 30 | 0.27 | 1143.9 | | 680.6 |
| | 35 | 0.31 | 865.3 | | 668.3 |
| | 40 | 0.55 | 538.9 | | 320.7 |
| HP-$\beta$-CD | 25 | 0.30 | 503.4 | 0.9612 | 501.3 |
| | 30 | 0.49 | 459.4 | | 459.5 |
| | 35 | 0.63 | 427.2 | | 427.3 |
| | 40 | 1.08 | 393.9 | | 391.8 |
| $\gamma$-CD | 25 | 0.26 | 342.6 | 9849 | 342.8 |
| | 30 | 0.33 | 332.2 | | 331.6 |
| | 35 | 0.41 | 327.9 | | 327.2 |
| | 40 | 0.64 | 308.6 | | 309.1 |

The $K_{1:1}$ values were 1350.7, 166.3, 120.0 and 652.0 M$^{-1}$ for $\beta$-CD, $\alpha$-CD, $\gamma$-CD, and HP-$\beta$-CD, respectively (Table 1). The low K1:1 values in the case of $\alpha$- and $\gamma$-CD are most likely due to two factors: (a) they are highly soluble in water, thus reducing the driving force for generation of a complex with BMTZ, and (b) $\alpha$-CD as a small cavity size that reduces the probability of including the large classes of BMTZ while $\gamma$-CD has a large cavity size that reduces effective interactions with BETA (Boyd et al., 2019). The differences obtained in the complexation of BMTZ with $\alpha$-, $\beta$- and $\gamma$-CD substantiated the significance of the aperture size in achieving a suffi-

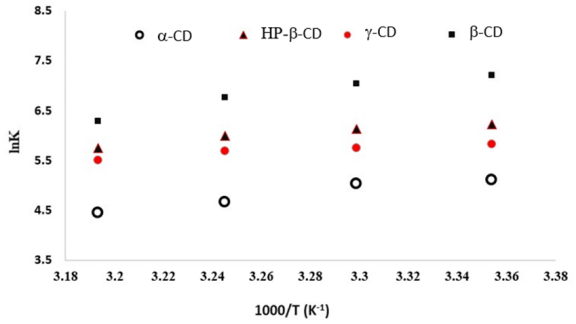


Figure 3: Plots depicting the development of BMTZ/CD complexes by Van't Hoff.

cient connection between host and guest molecules. The size of the 1:1 complexation constant for betamethasone, $K_{1:1}$, increased $\gamma$-CD<$\alpha$-CD<HP-$\beta$-CD«$\beta$-CD, clearly indicating the aperture of CDs. BMTZ formed the toughest complex with $\beta$-CD compared to other CDs (Table 1). BMTZ/$\beta$-CD complex was chosen for further investigation as shown below.

### 3.2 Physical mixture preparation (PM)

Physical mixtures of BMTZ and $\beta$-CD were prepared by mixing squashed powder of each component, which had previously been treated separately as it pertains to complex preparations employing the same complex stoichiometric molar ratio.

The solubility of BMTZ increased with increase in temperature. The solubility constant decreased with increase in temperature. Similarly, the size of the 1:1 complexation constants for the BMTZ, $K_{1:1}$ increased $\gamma$-CD<$\alpha$-CD<HP-$\beta$-CD«$\beta$-CD at the same temperature, clearly indicating the cavity of CDs.

### 3.3 Thermodynamics

The thermodynamics parameters, enthalpy change ($\Delta$H°) and entropy change ($\Delta$S°) for BMTZ/CD inclusion complex, were computed employing Van't Hoff equation:

$$\ln K = -\frac{\Delta H^\circ}{RT} + \frac{\Delta S^\circ}{R} \tag{2}$$

The slope and intercept from a plot of $\ln K$ against $1/T$ (Fig. 3) was employed to compute the $\Delta H^\circ$ and $\Delta S^\circ$ complex formation. Gibbs free energy change ($\Delta G^\circ$) was calculated in conformity with the equation:

$$\Delta G^\circ = \Delta H^\circ - T\Delta S^\circ \tag{3}$$

The inclusion complexation of CDs with BMTZ are mainly driven by non-covalent interactions forces such as Van der Waals, electrostatic, charge transfer, hydrophobic interplay as well as hydrogen bonding. $\Delta H^\circ$ and $\Delta S^\circ$ are negative for the generation of BETA/CD complexes. The high enthalpy values may suggest that the hydrogen bonds between BETA and CD in the generation of the complexes as well as the negative entropy changes could be associated with an orderly increase in the system when complexation occurs.

$\Delta H^\circ$ and $\Delta S^\circ$ are negative for the generation of BETA/CD complexes. The high enthalpy values may suggest that the hydrogen bonds between BETA and CD in the generation of the complexes as well as the negative entropy changes could be associated with an orderly increase in the system when complexation occurs. Consistent with the enthalpy–entropy compensation theory (Inoue et al., 1993a,b; Lewis and Hansen, 1973), the gain of enthalpy in the synthesis of inclusion compounds is achieved with decrease in entropy (Nakamura et al., 1995). The negative enthalpy change in these complexes discloses the presence of hydrophobic interaction (Bergeron, 1984; Srividya et al., 1996) in the BETA–CD systems.

Table 2: Values of $K_{1:1}$ and $K_{app}$ of the BMTZ/CD system achieved in 0.1 M phosphate buffer (pH 7.0) and varied temperatures.

| Complex | $\Delta H$ (kJ/mol) | $\Delta S$ (J/mol·K) | $\Delta G^\circ$ (kJ/mol) |
|---|---|---|---|
| BMTZ/$\beta$-CD | -44.64 | -89.04 | -18.09 |
| BMTZ/HP-$\beta$-CD | -24.14 | -28.94 | -15.51 |
| BMT/$\gamma$-CD | -16.46 | -6.51 | -14.52 |
| BMTZ/$\alpha$-CD | -36.84 | -78.06 | -13.57 |

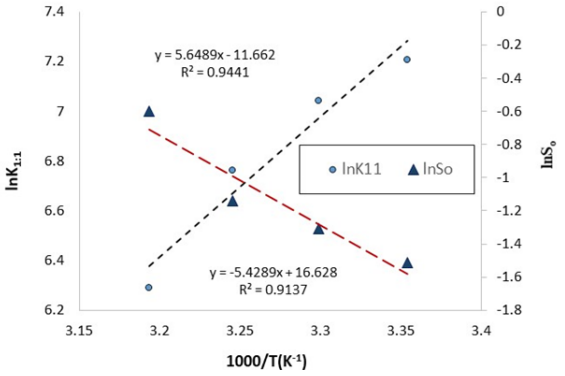


Figure 4: Graph of $\ln K_{1:1}$ and $\ln S_o$ against $1/T$.

In contrast to the constancy or stability constant, the solubility of BMTZ rose as the temperature was raised. Van't Hoff plots of $\ln K_{1:1}$ versus $1/T$ for BMTZ/CD complexes are reasonably linear; these figures are presented in Table 2. A 1:1 complex generation with CDs was observed.

Figure 4 depicts plots of $\ln K_{1:1}$ and $\ln S_o$ against $1/T$ for BMTZ/$\beta$-CD complex.

### 3.4 Characterization of BMTZ/$\beta$-CD solid complex

#### 3.4.1 Differential Scanning Calorimetry (DSC)

From the DSC, different types of information such as crystallization, thermal stability, melting etc. can be acquired on chemical compounds (Roy et al., 2016). DSC can be utilized for the recognition of inclusion complexes. In scenarios where the guest molecules were embedded in CD cavities, their melting, boiling or sublimation points mainly fluctuated among disparate temperatures or vanished. The DSC thermogram of BMTZ with $\beta$-CD shows an endothermic peak at 250 °C in DCS thermogram of

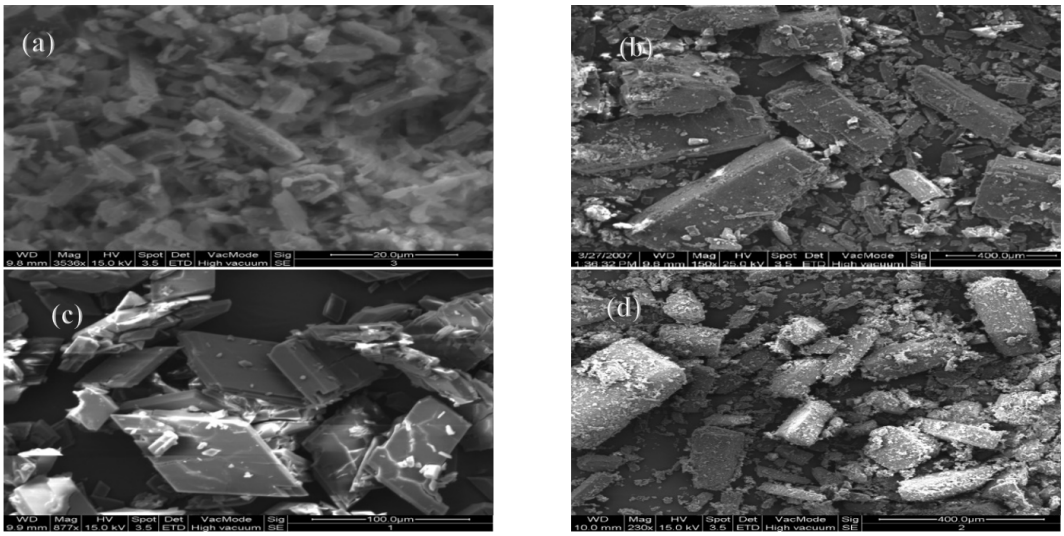


Figure 5: SEM photographs of (a) BMTZ (b) $\beta$-CD (c) BMTZ/$\beta$-CD inclusion complex (d) BMTZ/$\beta$-CD physical mixture.

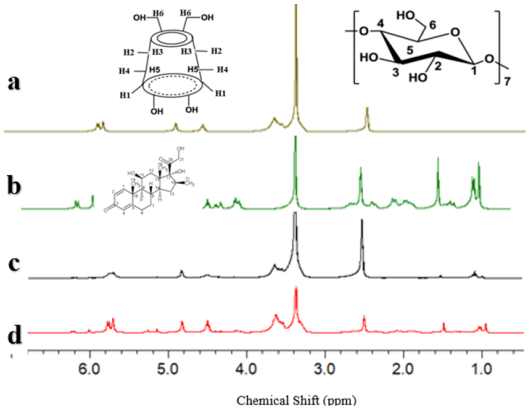


Figure 6: $^1$H NMR spectra of (a) $\beta$-CD, (b) BMTZ, (c) BMTZ/$\beta$-CD inclusion complex and (d) BMTZ/$\beta$-CD physical mixture.

BMTZ molecule (A) corresponds to betamethasone melting point. This peak also appeared in the physical mixture (B), but shifted to a small value, and vanished completely in the complex (C). This fact proves that complexes can form in the solid state.

### 3.4.2 Scanning electron microscope (SEM)

Figure 5 presents SEM images of BMTZ, $\beta$-CD, physical mixture and inclusion complex. Betamethasone is clearly aplatelike crystal with $\beta$-CD rhob-shaped crystals. Conversely, BETA/$\beta$-CD inclusion complex has a parallegram shape. In the inclusion complex, the unique architecture of the raw materials vanished, making it impracticable to distinguish between the two constituents.

### 3.4.3 $^1$H-NMR

$^1$H-NMR study was executed to elucidate the process of interaction of protons of BMTZ with the hydrophobic cavity of $\beta$-CD (Fig. 5). Since $\beta$-CD has a hydrophobic aperture which may encapsulate hydrophobic molecule BMTZ, the hydrogen bonding interactions between them may provide a momentum for the development of BMTZ/$\beta$-CD complex. If inclusion occurs, the transformations in both the physical and chemical environment will indubitably affect the density of electrons of hydrogens in BMTZ and $\beta$-CD. The number of chemical shifts, $\delta$ for different protons in both $\beta$-CD and BMTZ with inclusion complex (Fig. 6a, b, c) are presented in Tables 3 and 4. These chemical shifts are readily noticeable for protons situated at the CDs' internal surface (H-3 and H-5), however, it is very challenging to notice the chemical shifts of protons (H-1, H-2 and H-4) stationed at the CDs' superficial surface. The transformations in chemical shift ($\Delta\delta$) of H3 and H5 occurred owing to the BMTZ encapsulated in the hydrophobic aperture of $\beta$-CD and not because of non-bonded interactions between BMTZ and $\beta$-CD molecules.

Table 3: $^1$H-chemical shifts ($\delta$) of $\beta$-CD without and with BMTZ.

| $\beta$-CD protons | $\delta_{free}$ (ppm) | $\delta_{complex}$ (ppm) | $\Delta\delta$ (ppm) |
|---|---|---|---|
| H-1 | 4.829 | 4.829 | 0 |
| H-3 | 3.538 | 3.538 | 0 |
| H-6, 6' | 3.627 | 3.629 | -0.002 |
| H-5 | 3.366 | 3.364 | +0.002 |
| H-4 | 3.604 | 3.629 | -0.025 |
| H-2 | 3.571 | 3.574 | -0.003 |

BMTZ spectra, $\beta$-CD, physical mixture and inclusion complex were investigated to elucidate the possible interplay between host and guest.

However, as can be seen in Figure 6d, BMTZ and $\beta$-CD physical mixture did not show clear chemical shift changes at the corresponding hydrogen atom positions, indicating that no significant interaction occurred between BMTZ and $\beta$-CD in solid condition.

Table 4: $^1$H-chemical shifts ($\delta$) of BMTZ without and with of $\beta$-CD.

| BMTZ protons | $\delta_{free}$ (ppm) | $\delta_{complex}$ (ppm) | $\Delta\delta$ (ppm) |
|---|---|---|---|
| H-1 | 7.264 | 7.297 | -0.033 |
| H-2, 4 | 6.234 | 6.232 | 0.002 |
| | 6.011 | 6.012 | -0.001 |
| H-6, 6' | 1.869 | 1.872 | -0.003 |
| | 2.314 | 2.371 | -0.057 |
| OH-11 | 5.253 | 5.262 | -0.009 |
| OH-17 | 5.141 | 5.146 | -0.005 |
| H-21 | 4.341 | 4.336 | 0.005 |
| | 4.162 | 4.151 | 0.011 |
| OH-21 | 4.529 | 4.495 | 0.034 |

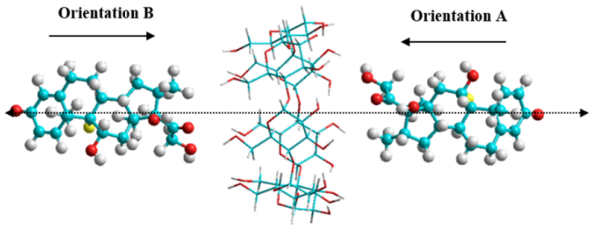


Figure 7: Coordinate structures for the 1:1 BMTZ complexation process with CD employing A and B guest–host orientation.

#### 3.4.4 Molecular modeling investigation of BMTZ/CD inclusion complexes

The BMTZ was docked to the CD molecules in order to determine their preferred binding configurations. There are two possible orientations (A and B) for the BMTZ molecule encapsulated in the hydrophobic aperture of the CD as illustrated in Fig. 7. In orientation A, the C=O groups point toward the secondary CD rim, but in orientation B, the opposite is the case.

The binding energies were estimated and tabulated in Table 5 utilizing the relation:

$$E_{binding} = E_{BMTZ/CD\ complex} - (E_{isolated\ BMTZ} + E_{isolated\ CD}) \quad (4)$$

The employment of multiple replica compounds in the parameterization procedures of these force fields explains why different force fields can predict varied binding energy values for the same system and methodology. The binding energy values were in the range from -26.6 kcal/mol (case of BMTZ/$\alpha$-CD) to -54.0 kcal/mol (case of BMTZ/HP-$\beta$-CD) for Amber force field (Table 5), indicating that complex formation is thermodynamically favored. Approach B was found more favored than approach A in all complex cases. The utmost robust complex yielded 100 % BMTZ in the $\beta$-CD, $\gamma$-CD and HP-$\beta$-CD cavities. These inclusion modes are characterized by the interaction of the "hydroxyacetyl" group of the guest with atoms of the narrow CD rims, while the opposite guest side (cyclohexa-2, 5-dien-1-one) interacts with atoms of the wide rim of the hosts. The conformation of the 1:1 complex with BMTZ/$\alpha$-CD are presented in Fig. 8c. Only the hydroxyacety portion of the complex can be seen partially inserted into the aperture of the CD.

## 4. Conclusions

The outcomes of this investigation revealed that the BMTZ formed 1:1 type complexes with all examined CDs. The phase solubility experiment indicated that BMTZ/$\beta$-CD complex had a $B_s$-type curve, whereas other CDs had an $A_L$-type curve. The Van't Hoff equation was employed to compute the thermodynamic parameters. The negative values associated with changes in enthalpy and entropy suggest that the production of the above-mentioned complexes is induced by both enthalpy and entropy. All the data obtained from phase solubility, SEM, DSC and NMR studies along with MM modeling provide strong indications of the formation of very stable inclusion complexes between BMTZ and native and modified CDs. The inclusion model forecasted through experimental investigations agrees well with the actively advantageous complex acquired from molecular docking examinations. As a result, the inclusion complex of BMTZ with CDs can be employed as a new strategy to enhance BMTZ's physical and chemical properties for better oral bioavailability.

## 5. Acknowledgments

We appreciate the financial support from Al al-Bayt University's graduate studies faculty and the Deanship of Scientific Research.

## 6. Funding details

This study was supported by the Scientific and Technical Research Council of Turkiye [TUBITAK, 119R001].

## References

Agirman, B. (2014). *Reducing sodium chloride amount by using different chloride salts in shalgam juice production.* Cukurova University, Turkey.

Al-Sou'od, K. A. (2008). Investigation of the hydrocortisone-$\beta$-cyclodextrin complex by phase solubility method: Some theoretical and practical considerations. *Journal of Solution Chemistry*, 37(1):119–133.

Anli, R. E., Vural, N., Demiray, S., and Mert, B. (2006). Biogenic amine content of beers consumed in Turkey and influence of storage conditions on biogenic amine formation. *Journal of the Institute of Brewing*, 112(3):267–274.

Anonymous (2022). *The good scents company information system.* (accessed February 17, 2022).

Bergeron, R. (1984). Inclusion Compounds. Academic Press, New York, USA.

Bonneau, A., Boulanger, R., Lebrun, M., Maraval, I., and Gunata, Z. (2016). Aroma compounds in fresh and dried mango fruit (Mangifera indica L. cv. Kent): Impact of drying on volatile composition. *International Journal of Food Science & Technology*, 51(3):789–800.

Boyd, B. J., Bergström, C. A., Vinarov, Z., Kuentz, M., Brouwers, J., Augustijns, P., Brandl, M., Bernkop-Schnürch, A., Shrestha, N., Préat, V., Müllertz, A., Bauer-Brandl, A., and Jannin, V. (2019). Successful

Table 5: Binding energies (kJ·mol$^{-1}$) of optimal BMTZ/CD complex geometries.

| Guest | Approach | $MM_{bond\ dipoles}$ | $MM_{atomic\ charges}$ | Amber kcal/mol | BIO+ | OPLS |
|---|---|---|---|---|---|---|
| $\beta$-CD | A | -29.9 | -31.6 | -42.3 | -31.6 | -38.6 |
| | B | -35.2 | -28.3 | -44.4 | -33.6 | -43.0 |
| $\gamma$-CD | A | -24.4 | -25.6 | -32.8 | -28.4 | -30.3 |
| | B | -27.8 | -24.1 | -34.9 | 29.5 | -31.1 |
| $\alpha$-CD | A | -22.5 | -19.9 | -26.6 | -21.1 | -22.7 |
| | B | -23.1 | -20.3 | -28.8 | -21.9 | -24.0 |
| HP-$\beta$-CD | A | -39.5 | -36.8 | -48.7 | -45.3 | -47.9 |
| | B | -44.5 | -41.0 | -54.0 | -41.9 | -55.5 |

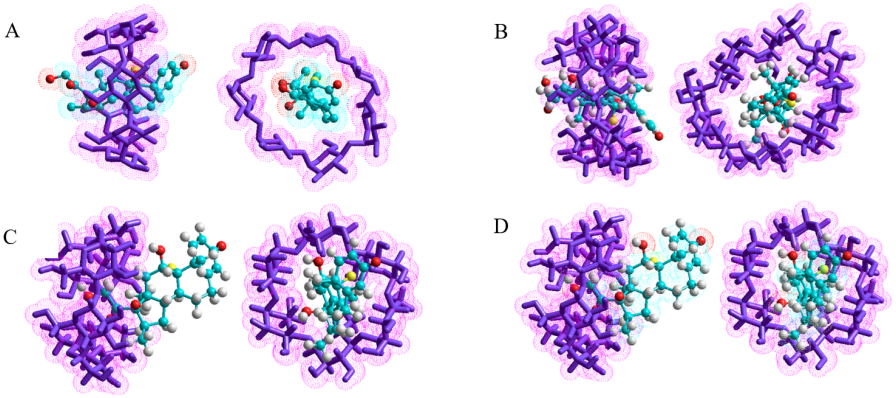


Figure 8: The most favorable 1:1 inclusion complexes arrangements (A) BMTZ/$\beta$-CD and (B) BMTZ/$\gamma$-CD (C) BMTZ/$\alpha$-CD (D) BMTZ/HP-$\beta$-CD.

oral delivery of poorly water-soluble drugs both depends on the intraluminal behavior of drugs and of appropriate advanced drug delivery systems. *European Journal of Pharmaceutical Sciences*, 137:104967.

Cankaya, A. (2018). *The effect of different fermentation temperature and production method on antioxidant activity, anthocyanin and phenolic compounds of turnip juice*. Niğde University, Turkey.

Cheng, C. J., Tietjen, G. T., Saucier-Sawyer, J. K., and Saltzman, W. M. (2015). A holistic approach to targeting disease with polymeric nanoparticles. *Nature Reviews Drug Discovery*, 14(4):239–247.

Cirak, M. (2016). *The effect of different fermentation temperature application on quality of shalgam production*. Cukurova University, Turkey.

Colak, H. and Ugur, M. (2002). The effect of different temperature and time in storage on the formation of biogenic amines in fermented sucuks. *Turkish J. Vet. Anim. Sci.*, 26:779–784.

Dai, Y., Zhong, J., Li, J., Liu, X., Wang, Y., and Qin, X. (2022). Interaction mechanism of cholesterol/$\beta$-cyclodextrin complexation by combined experimental and computational approaches. *Food Hydrocolloids*, 130:107725.

Flood, K. G., Reynolds, E. R., and Snow, N. H. (2000). Characterization of inclusion complexes of betamethasone-related steroids with cyclodextrins using high-performance liquid chromatography. *Journal of Chromatography A*, 903(1-2):49–65.

Gillet, A., Grammenos, A., Compère, P., Evrard, B., and Piel, G. (2009). Development of a new topical system: Drug-in-cyclodextrin-in-deformable liposome. *International Journal of Pharmaceutics*, 380(1-2):174–180.

Gunes, G. (2008). *Research on the determination of the most appropriate black carrot amount in shalgam juice production*. Cukurova University, Turkey.

Inoue, Y., Hakushi, T., Liu, Y., Tong, L., Shen, B., and Jin, D. (1993a). Thermodynamics of molecular recognition by cyclodextrins. 1. Calorimetric titration of inclusion complexation of naphthalenesulfonates with $\alpha$-, $\beta$-, and $\gamma$-cyclodextrins: enthalpy-entropy compensation. *Journal of the American Chemical Society*, 115(2):475–481.

Inoue, Y., Liu, Y., Tong, L. H., Shen, B. J., and Jin, D. S. (1993b). Calorimetric titration of inclusion complexation with modified. beta-cyclodextrins. Enthalpy-entropy compensation in host-guest complexation: from ionophore to cyclodextrin and cyclophane. *Journal of the American Chemical Society*, 115(23):10637–10644.

Jansook, P., Ogawa, N., and Loftsson, T. (2018). Cyclodextrins: Structure, physicochemical properties and pharmaceutical applications. *International Journal of Pharmaceutics*, 535(1-2):272–284.

Kebede, B. T., Grauwet, T., Palmers, S., Vervoort, L., Carle, R., Hendrickx, M., and Van Loey, A. (2014). Effect of high pressure high temperature processing on the volatile fraction of differently coloured carrots. *Food Chemistry*, 153:340–352.

Keskin, M., Guclu, G., Sekerli, Y. E., Soysal, Y., Selli, S.,

and Kelebek, H. (2021). Comparative assessment of volatile and phenolic profiles of fresh black carrot (Daucus carota L.) and powders prepared by three drying methods. *Scientia Horticulturae*, 287:110256.

Kirlangic, O., Ilgaz, C., and Kadiroglu, P. (2021). Influence of pasteurization and storage conditions on microbiological quality and aroma profiles of shalgam. *Food Biosci.*, 44(101350).

Lewis, E. A. and Hansen, L. D. (1973). Thermodynamics of binding of guest molecules to $\alpha$- and $\beta$-cyclodextrins. *J. Chem. Soc., Perkin Trans. 2*, (15):2081–2085.

Maifreni, M., Marino, M., and Conte, L. (2004). Lactic acid fermentation of Brassica rapa: Chemical and microbial evaluation of a typical Italian product (brovada). *European Food Research and Technology*, 218(5):469–473.

Malaekeh-Nikouei, B., Nassirli, H., and Davies, N. (2007). Enhancement of cyclosporine aqueous solubility using $\alpha$- and hydroxypropyl $\beta$-cyclodextrin mixtures. *Journal of Inclusion Phenomena and Macrocyclic Chemistry*, 59(3-4):245–250.

Miao, J., Guo, Z., Wang, Y., Chen, D., Li, Y., and Zhang, F. (2017). Study on the inclusion complex between $\beta$-cyclodextrin derivatives and flurbiprofen by spectrofluorometric. In *AIP Conference Proceedings*.

Misiuk, W. and Zalewska, M. (2009). Investigation of inclusion complex of trazodone hydrochloride with hydroxypropyl-$\beta$-cyclodextrin. *Carbohydrate Polymers*, 77(3):482–488.

Molina, A. M., Guadalupe, V., Varela, C., Swiegers, J. H., Pretorius, I. S., and Agosin, E. (2009). Differential synthesis of fermentative aroma compounds of two related commercial wine yeast strains. *Food Chemistry*, 117(2):189–195.

Molina, A. M., Swiegers, J. H., Varela, C., Pretorius, I. S., and Agosin, E. (2007). Influence of wine fermentation temperature on the synthesis of yeast-derived volatile aroma compounds. *Applied Microbiology and Biotechnology*, 77(3):675–687.

Nakamura, A., Sato, S., Hamasaki, K., Ueno, A., and Toda, F. (1995). Association of 1:1 inclusion complexes of cyclodextrins into homo- and heterodimers: A spectroscopic study using a TICT-forming fluorescent probe as a guest compound. *Journal of Physical Chemistry*, 99(27):10952–10959.

Otagiri, M., Fujinaga, T., A., S., and Uekama, K. (1984). Effects of $\beta$- and $\gamma$-cyclodextrins on release of betamethasone from ointment bases. *Chemical and Pharmaceutical Bulletin*, 32(6):2401–2405.

Özdestan, Ö. and Üren, A. (2010). Biogenic amine content of Shalgam (Şalgam): A traditional lactic acid fermented Turkish beverage. *Journal of Agricultural and Food Chemistry*, 58(4):2602–2608.

Ozturk, O. (2009). *Research on the composition of shalgam beverages obtained from Adana Market*. Cukurova University, Turkey.

Piel, G., Piette, M., Barillaro, V., Castagne, D., Evrard, B., and Delattre, L. (2006). Betamethasone-in-cyclodextrin-in-liposome: The effect of cyclodextrins on encapsulation efficiency and release kinetics. *International Journal of Pharmaceutics*, 312(1-2):75–82.

Ravishankar, K. and Dhamodharan, R. (2020). Advances in chitosan-based hydrogels: Evolution from covalently crosslinked systems to ionotropically crosslinked superabsorbents. *Reactive and Functional Polymers*, 149:104517.

Srividya, N., Ramamurthy, P., Shanmugasundaram, P., and Ramakrishnan, V. T. (1996). Synthesis, characterization, and electrochemistry of some acridine-1,8-dione dyes. *The Journal of Organic Chemistry*, 61(15):5083–5089.

Szejtli, J. (1998). Introduction and general overview of cyclodextrin chemistry. *Chem. Rev.*, 98:1743–1754.

Tanguler, H., Selli, S., Sen, K., Cabaroglu, T., and Erten, H. (2017). Aroma composition of shalgam: a traditional Turkish lactic acid fermented beverage. *Journal of Food Science and Technology*, 54(7):2011–2019.

Taveira, M., Fernandes, F., Guedes de Pinho, P., Andrade, P. B., Pereira, J. A., and Valentão, P. (2009). Evolution of Brassica rapa var. rapa L. volatile composition by HS-SPME and GC/IT-MS. *Microchemical Journal*, 93(2):140–146.

Torres, S., Roeckel, M., and Marti, M. (2002). Histamine formation by Morganella morganii iso-lated from Trachurus murphyii (Chilean mackerel). *Latin American Applied Research*, 32(2):209–214.

TSE (2003). *TS 11149 Standard of Shalgam Beverage*. Turkish Standards Institute, TSE, Ankara, Turkey.

Uria-Canseco, E., Perez-Casas, S., and Navarrete-Vázquez, G. (2019). Thermodynamic characterization of the inclusion complexes formation between antidiabetic new drugs and cyclodextrins. *The Journal of Chemical Thermodynamics*, 129:55–60.

Utus, D. (2008). *The effect of black carrot (Daucus carota) size used on the quality of shalgam production*. Cukurova University, Turkey.

Welke, J. E., Nicolli, K. P., Hernandes, K. C., Biasoto, A. C. T., and Zini, C. A. (2022). Adaptation of an olfactometric system in a GC-FID in combination with GCxGC/MS to evaluate odor-active compounds of wine. *Food Chemistry*, 370:131004.

Zughul, M. and Badwan, A. (1998). $SL_2$ type phase solubility diagrams, complex formation and chemical speciation of soluble species. *J. Incl. Phenom. Macrocyclic Chem.*, 31:243–264.

Zughul, M. B. (2007). Rigorous nonlinear regression analysis of phase solubility diagrams to obtain complex stoichiometry and true thermodynamic drug-cyclodextrin complexation parameters. *Journal of Inclusion Phenomena and Macrocyclic Chemistry*, 57(1-4):525–530.